

See discussions, stats, and author profiles for this publication at: <https://www.researchgate.net/publication/274318037>

# Cobalt Nanoparticles Embedded in Nitrogen-Doped Carbon for the Hydrogen Evolution Reaction

ARTICLE in ACS APPLIED MATERIALS & INTERFACES · MARCH 2015

Impact Factor: 6.72 · DOI: 10.1021/acsaami.5b00652 · Source: PubMed

---

CITATIONS

3

READS

45

## 8 AUTHORS, INCLUDING:



Yang Yang

Rice University

43 PUBLICATIONS 638 CITATIONS

[SEE PROFILE](#)



Zhiwei Peng

University of Maryland, College Park

49 PUBLICATIONS 1,480 CITATIONS

[SEE PROFILE](#)



Lei Li

New York State Department of Health

32 PUBLICATIONS 618 CITATIONS

[SEE PROFILE](#)

# Cobalt Nanoparticles Embedded in Nitrogen-Doped Carbon for the Hydrogen Evolution Reaction

Huilong Fei,<sup>†</sup> Yang Yang,<sup>†,‡</sup> Zhiwei Peng,<sup>†</sup> Gedeng Ruan,<sup>†</sup> Qifeng Zhong,<sup>†</sup> Lei Li,<sup>†</sup> Errol L. G. Samuel,<sup>†</sup> and James M. Tour<sup>\*,†,‡,§</sup>

<sup>†</sup>Department of Chemistry, <sup>‡</sup>Smalley Institute for Nanoscale Science and Technology, <sup>§</sup>Department of Materials Science and NanoEngineering, Rice University, 6100 Main Street, Houston, Texas 77005, United States

## Supporting Information

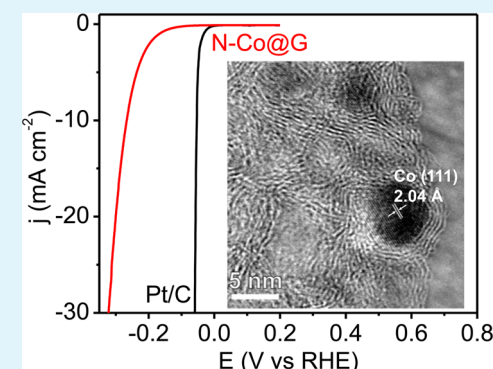
**ABSTRACT:** There is great interest in renewable and sustainable energy research to develop low-cost, highly efficient, and stable electrocatalysts as alternatives to replace Pt-based catalysts for the hydrogen evolution reaction (HER). Though nanoparticles encapsulated in carbon shells have been widely used to improve the electrode performances in energy storage devices (e.g., lithium ion batteries), they have attracted less attention in energy-related electrocatalysis. Here we report the synthesis of nitrogen-enriched core–shell structured cobalt–carbon nanoparticles dispersed on graphene sheets and we investigate their HER performances in both acidic and basic media. These catalysts exhibit excellent durability and HER activities with onset overpotentials as low as ~70 mV in both acidic (0.5 M H<sub>2</sub>SO<sub>4</sub>) and alkaline (0.1 M NaOH) electrolytes, and the overpotentials needed to deliver 10 mA cm<sup>-2</sup> are determined to be 265 mV in acid and 337 mV in base, further demonstrating their potential to replace Pt-based catalysts. Control experiments reveal that the active sites for HER might come from the synergistic effects between the cobalt nanoparticles and nitrogen-doped carbon.

**KEYWORDS:** *electrocatalytic hydrogen evolution, nitrogen doping, graphene, cobalt nanoparticles, synergistic effects*

## ■ INTRODUCTION

Hydrogen is proposed as a promising energy carrier in our energy landscape since it is oxidized to water, it has a high gravimetric energy density, and it is renewable.<sup>1,2</sup> Electrolysis of water has been widely investigated as a sustainable method to produce H<sub>2</sub> fuel through the hydrogen evolution reaction (HER). The efficiency of HER relies on the use of high-performance electrocatalysts; Pt-based catalysts remain the most effective for this purpose.<sup>3</sup> However, the scarcity and high cost of Pt limits its commercialization and widespread use.<sup>4</sup> This fact has led to extensive research into developing efficient and less expensive alternatives using non-noble-metal electrocatalysts. For example, layered transition-metal dichalcogenides (MoS<sub>2</sub>,<sup>5,6</sup> WS<sub>2</sub>,<sup>4,7</sup> MoSe<sub>2</sub>,<sup>8</sup> WSe<sub>2</sub>,<sup>9</sup>), first-row transition-metal dichalcogenides (CoS<sub>2</sub>,<sup>10,11</sup> CoSe<sub>2</sub>,<sup>12</sup>), metal phosphide (CoP,<sup>13,14</sup> NiP,<sup>15,16</sup> Cu<sub>3</sub>P,<sup>17</sup> MoP,<sup>18</sup>), carbide (MoC,<sup>19,20</sup> WC,<sup>21</sup>), boride (Ni<sub>2</sub>B,<sup>22</sup> MoB,<sup>19</sup>), nitride (W<sub>2</sub>N,<sup>23</sup> Co<sub>0.8</sub>Mo<sub>1.4</sub>N<sub>2</sub>,<sup>24</sup>), and carbon-based compounds (C<sub>3</sub>N<sub>4</sub>@NG,<sup>25</sup> N,P-graphene,<sup>26</sup>) all have been reported to be promising HER electrocatalysts.

Transition-metal-containing nanoparticles (NPs) encapsulated in carbon layers have been used in the design of advanced electrode (anode and cathode) materials with improved rate capability and cycling life for energy storage in lithium ion batteries.<sup>27–30</sup> This is mainly because conductive carbon layers can provide efficient electron transport paths while suppressing the pulverization problem during the battery charge–discharge



process.<sup>31,32</sup> However, only very recently have transition-metal nanoparticles in carbon layers found application in the field of energy-related electrocatalysis. For example, Hu et al. found that iron carbide NPs encased in graphite layers were highly active electrocatalysts for the oxygen reduction reaction (ORR) in both acid and alkaline electrolytes.<sup>33</sup> Wen et al. reported the use of nitrogen-enriched core–shell structured catalysts with Fe/Fe<sub>3</sub>C nanorods as the core and graphite carbon as the shell for ORR with improved activities and kinetics in neutral electrolyte.<sup>34</sup> More recently, there were two works reported using Co or FeCo alloy NPs embedded in nitrogen-doped carbon nanotubes as highly efficient catalyst for HER, and they can be used over wide pH ranges.<sup>35–38</sup> These catalysts represent an interesting category of heterogeneous catalysts where the metals are not in direct contact with the electrolyte, but can influence the protective carbon layer toward catalytic processes. Though there is still a lack of thorough understanding on the electrocatalytically active sites, it is proposed that the catalytic activity might come from the structural and electronic interaction between the metal cores and the carbon shells.<sup>33,39</sup> This interaction can be adjusted by changing the metal core composition, the carbon layer thickness, or by doping carbon with heteroatoms.<sup>40–42</sup> Hence, various degrees

**Received:** January 21, 2015

**Accepted:** March 31, 2015

**Published:** March 31, 2015



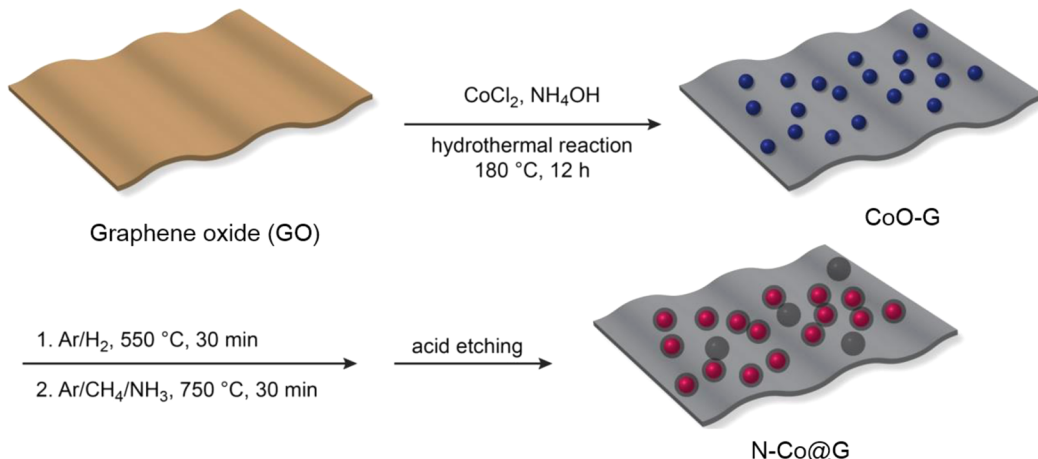


**Figure 1.** Illustration of the preparation procedure for the N-Co@G nanocomposites.

of freedom are rendered for tuning the catalytic properties in metal particles with carbon shells.<sup>39,43</sup>

Here we report the synthesis of nitrogen-enriched carbon-encapsulated cobalt NPs dispersed on graphene sheets (N-Co@G). The Co NPs are small in size (<10 nm) and are in intimate contact with the nitrogen-enriched carbon, which can provide numerous catalytically active sites. In addition, these NPs are further interconnected by graphene sheets with macroporous structure formed during a hydrothermal synthesis process, which can facilitate electron and mass transport during catalytic tests. As a result, this N-Co@G nanocomposite can serve as a highly efficient and durable HER electrocatalyst under both acidic and basic conditions, which is valued properties for HER catalysts.<sup>19</sup> The onset overpotentials are as low as ~70 mV in both acid and alkaline solutions, and the overpotentials needed to deliver 10 mA cm<sup>-2</sup> are 265 mV in acid and 337 mV in base, respectively.

## RESULTS AND DISCUSSION

The preparation route of N-Co@G is shown in Figure 1. First, a suspension mixture of graphene oxide (GO), CoCl<sub>2</sub> and NH<sub>4</sub>OH was hydrothermally treated at 180 °C for 12 h. This method is a well-known, simple and versatile approach to fabricate three-dimensional (3D) graphene/metal oxide hybrids.<sup>44</sup> After freeze-drying, the morphology of this product was characterized by scanning electron microscopy (SEM) and transmission electron microscopy (TEM) and it can be seen that the graphene sheets are interconnected to form macroporous frameworks and the surfaces of the graphene sheets are decorated with small crystalline CoO nanocrystals (<10 nm) (denoted as CoO-G) (Figure S1). The CoO-G was then subjected to a two-step chemical vapor deposition (CVD) process. In the first step, the CoO nanocrystals were reduced in a H<sub>2</sub> atmosphere at 550 °C for 30 min to form metallic Co, which is then used as a catalyst to grow carbon shells in the following step. CH<sub>4</sub> was used at 750 °C as a carbon source and NH<sub>3</sub> was introduced during the growth to dope N into the grown carbon shells as well as into the graphene sheets. Finally, the product after CVD growth was leached in 0.5 M H<sub>2</sub>SO<sub>4</sub> at 90 °C for 5 h to remove the exposed Co NPs to obtain the final product of N-Co@G.

SEM images (Figure 2a,b) show that the N-Co@G has a 3D macroporous structure and the graphene sheet surfaces are rough because of the decorated NPs. This was further

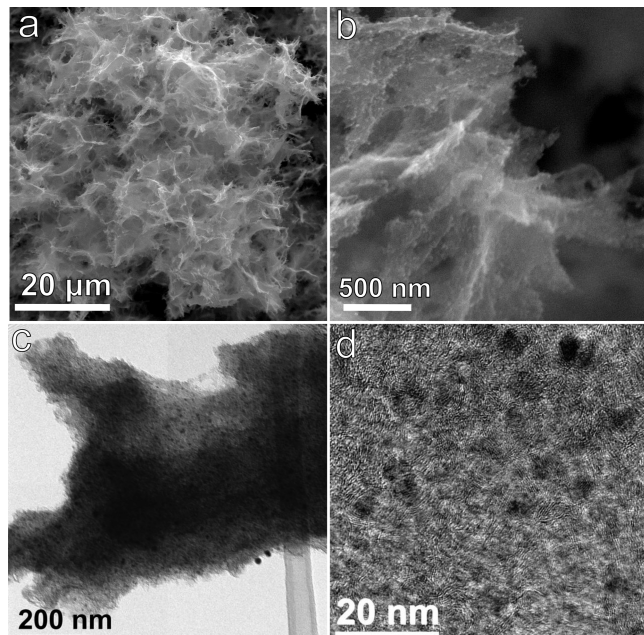


**Figure 2.** SEM images of N-Co@G at (a) low and (b) high magnifications. TEM images of N-Co@G at (c) low and (d) high magnifications.

confirmed by TEM observation at low magnification (Figure 2c), which shows that many small NPs (<10 nm) are uniformly dispersed on the graphene sheets. It worth noting here that after the CVD high temperature growth process, the NPs remain in their original size range with negligible aggregation. This is because the graphene sheets with their high thermal stability and large aspect ratio can act as excellent space restrictors that localize the Co nanoparticles to prevent their sintering at elevated temperatures.<sup>45</sup> The high magnification TEM image (Figure 2d) shows that each individual NP is coated by thin carbon shells (2 to 5 layers), and this becomes more clear by high resolution TEM (HRTEM) (Figure 3a). Also, some hollow carbon spheres can be observed that were formed during the leaching process on the residual poorly coated core-shell NPs. Further, Figure 3a shows that the NPs exhibit a *d* spacing of 2.04 Å, corresponding to the (111) plane of metallic Co.

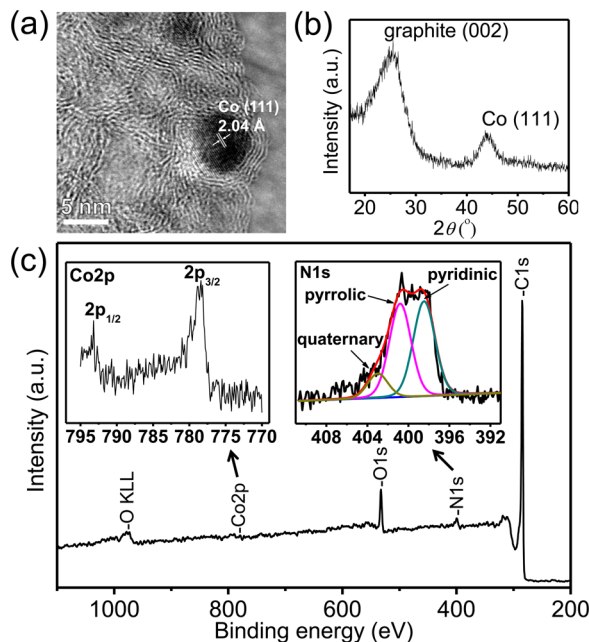


**Figure 3.** (a) HRTEM image of N-Co@G with the  $d$  spacing of the (111) plane indicated. (b) XRD pattern of N-Co@G, showing the characteristic peaks for graphite and metallic Co. (c) XPS survey spectra of N-Co@G with the insets showing the high resolution Co 2p and N 1s spectra.

The presence of metallic Co and crystalline carbon was further confirmed by X-ray diffraction (XRD) (Figure 3b), which shows the characteristic (002) plane peak for graphite and the (111) plane peak for metallic Co. The survey scan of X-ray photoelectron spectroscopy (XPS) analysis (Figure 3c) shows the characteristic peaks of C (91.6 at%), oxygen (5.6 at %), and N (2.8 at%). The peak for Co is negligible, as they are encapsulated in carbon shells and can only be observed by high resolution Co 2p spectra (Figure 3c, inset). The peak position of Co 2p<sub>3/2</sub> is at ~778.5 eV, further corroborating the metallic form of Co. The high resolution N 1s peak reveals that there are three different types of N species, with pyridinic (398.5 eV) and pyrrolic (400.8 eV) as a dominant and quaternary (402.8 eV) as the minor component.<sup>46</sup>

The electrocatalytic activity of N-Co@G toward HER was first evaluated in 0.5 M H<sub>2</sub>SO<sub>4</sub> electrolyte using a typical three-electrode system. The working electrode used was glassy carbon with an active material mass loading of 285  $\mu\text{g cm}^{-2}$ . For comparison, commercially available 20 wt % Pt on Vulcan carbon black (Pt/C from Alfa Aesar) with the same mass loading was also examined. Figure 4a shows polarization curves at 5 mV s<sup>-1</sup> after  $iR$  compensation, and Figure 4b shows the enlarged view near the onset potential region. As would be expected, the Pt/C electrode shows extraordinary HER activity with a near-zero onset overpotential. For the N-Co@G electrode, it exhibits a small onset overpotential of ~70 mV, upon which the cathodic current density increases rapidly at more negative potentials, and it takes 265 mV overpotential to deliver a current density of 10 mA cm<sup>-2</sup>. These results demonstrate that the N-Co@G is a highly active HER electrocatalyst and its activity compares favorably with the most active noble-metal-free HER catalysts in acidic solution (see Table S1). Electrochemical impedance spectra (EIS) (Figure S2) obtained at an open circuit potential show dominant capacitive behavior, indicating its good electrical

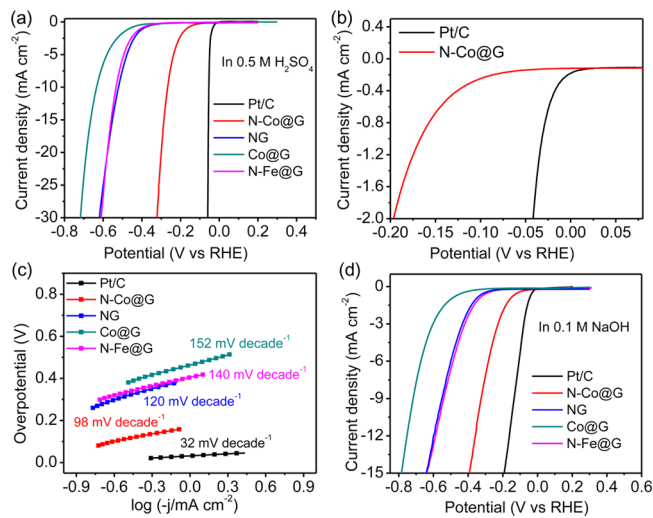


**Figure 4.** Electrochemical characterizations for HER activity. (a) Polarization curves obtained in 0.5 M H<sub>2</sub>SO<sub>4</sub> at 5 mV s<sup>-1</sup> for N-Co@G, NG, Co@G, and N-Fe@G along with commercial Pt/C for comparison. (b) Enlarged view of the polarization curves near the onset potential region for N-Co@G and Pt/C. (c) Tafel plots of the corresponding samples. (d) Polarization curves obtained in 0.1 M NaOH at 5 mV s<sup>-1</sup>.

conductivity. EIS performed at an overpotential of 200 mV gives a charge transfer resistance of  $\sim 270 \Omega$ . To estimate the electrochemically active surface area, we measured the double layer capacitance from the scan-rate dependence of cyclic voltammograms (CVs). The results (Figure S3) show that the N-Co@G electrode has a capacitance of 10 mF cm<sup>-2</sup> which corresponds to a surface roughness of  $\sim 285$ , assuming the capacitance for a flat electrode is 35  $\mu\text{F cm}^{-2}$ .<sup>47</sup> The high surface area of N-Co@G also contributes to its high catalytic activity.

To study the effect of Co and N on the HER activity, control samples of N-doped graphene without any Co (NG) and N dopant-free sample (Co@G) were prepared (see Experimental Section for details). The absence of Co in NG and of N in Co@G were confirmed by XPS (Figure S4). These control samples were then tested under the same conditions as N-Co@G. As can be seen in Figure 4a, NG has very low activity with an onset overpotential as large as  $\sim 240$  mV, consistent with other reports,<sup>25,26</sup> while the Co@G exhibits even poorer activity with  $\sim 350$  mV onset overpotential. These results suggest that the HER activity of N-Co@G comes from the synergistic effects between the Co and N dopants. To further illustrate the point that the Co nanoparticles have contributed to the observed HER activity of N-Co@G, the Co core was replaced with Fe by exchanging the CoCl<sub>2</sub> with FeCl<sub>2</sub> during the hydrothermal synthesis and then treating under the same synthetic conditions as those used for N-Co@G. The resultant product was denoted as N-Fe@G. The HER test results (Figure 4a) show that it has very poor activity, similar to NG, indicating that the Fe core contributes little to the HER activity. TEM, XPS and Raman characterizations (Figures S5–7) show that N-Fe@G has similar structural features, N content and N types, and degree of carbon crystallinity, so the observed difference in HER activity can only be ascribed to the different compositions of the metal core.

To understand the HER reaction mechanism that occurred in these catalysts, Tafel slopes were determined by fitting the

linear portions of the Tafel plots. The results are summarized in Figure 4c. The HER on Pt surfaces is known to proceed through the Volmer–Tafel mechanism and the second step is the rating-limiting reaction at low overpotentials.<sup>48</sup> This results in a Tafel slope of  $32 \text{ mV decade}^{-1}$  measured in this study. The Tafel slope for N-Co@G is  $98 \text{ mV decade}^{-1}$ , which indicates that HER on this catalyst may occur via the Volmer-Heyrovsky mechanism.<sup>36</sup> The Tafel slope values for the other control samples are much larger, at  $120$  to  $152 \text{ mV decade}^{-1}$ .

The high HER activity of N-Co@G is not only limited to acidic media. The electrochemical measurements performed in  $0.1 \text{ M NaOH}$  (Figure 4d and Figure S8) show that the N-Co@G exhibits excellent catalytic activity as well. In this alkaline electrolyte, its onset overpotential is  $\sim 70 \text{ mV}$ , which is similar in acidic electrolyte and only marginally larger than the near-zero value of the Pt/C electrode tested under the same conditions. The overpotential needed for the N-Co@G to deliver  $10 \text{ mA cm}^{-2}$  is determined to be  $337 \text{ mV}$ . These results indicate that N-Co@G is a highly active electrocatalyst toward HER in alkaline media and its activity is comparable to some of the best non-noble-metal catalysts for HER under basic solutions (Table S2). The high HER activity of the Co@G in alkaline electrolyte makes it complementary to the well-known MoS<sub>2</sub> catalyst, which is stable only in acidic electrolyte and MoS<sub>2</sub> application in alkaline electrolysis is limited.<sup>49</sup> The other control samples were also tested under the same alkaline conditions. The results show similar activity trends as in acid, with the N-G and N-Fe@G having similar polarization curves, and the Co@G having the poorest activity.

Besides activity, durability is another important requirement for good HER electrocatalysts to guarantee sustainable H<sub>2</sub> generation. Especially for the N-Co@G, its HER stability in acid might be a concern considering the fact that the Co metal, if not well-protected by the carbon shells, would gradually dissolve by the acidic electrolyte and thus the activity might degrade with cycling. To evaluate the long-term stability of the N-Co@G, continuous cyclic voltammetry was performed from  $0.3$  to  $-0.5 \text{ V}$  vs RHE at  $50 \text{ mV s}^{-1}$  under both basic and acidic conditions for 1000 cycles. The results (Figure 5) show that the

followed by a CVD process. The nitrogen can be easily incorporated into the carbon matrix by introducing a nitrogen precursor ( $\text{NH}_3$ ) during the growth of carbon shells. The nanoparticles are small in size ( $<10 \text{ nm}$ ) and evenly distributed on the graphene sheets. When tested as a HER electrocatalyst, the N-Co@G exhibits superior stability and HER activity with onset overpotentials of only  $\sim 70 \text{ mV}$  in both acid and base electrolytes, making it among the most active HER catalyst reported (Table S1 and S2). The HER active sites originate from the synergistic effects between the Co nanoparticles and N-doped carbon. This work shows the efficacy of precious-metal-free electrocatalysts for hydrogen evolution based on the interface between transition metal and heteroatom-doped carbon.

## EXPERIMENTAL SECTION

**Materials synthesis.** All chemicals were purchased from Sigma-Aldrich unless otherwise specified. Graphene oxide (GO) was synthesized from graphite flakes ( $\sim 150 \mu\text{m}$  flakes) using the improved Hummers method.<sup>50</sup>

**Synthesis of CoO-G.** Fifteen mg  $\text{CoCl}_2 \cdot 6\text{H}_2\text{O}$  was added into  $10 \text{ mL}$  GO aqueous suspension ( $3 \text{ mg mL}^{-1}$ ) and bath-sonicated (Cole Parmer, model 08849–00) for 30 min. Then,  $30 \mu\text{L}$   $\text{NH}_3 \cdot \text{H}_2\text{O}$  (28 wt %) was added to the mixture and sonicated for another 30 min. The suspension was sealed in a  $25 \text{ mL}$  Teflon-lined autoclave and hydrothermally treated at  $180^\circ\text{C}$  for 12 h. The CoO-G nanocomposite was obtained by freeze-drying of the product after hydrothermal reaction.

**Synthesis of N-Co@G.** CoO-G was placed in a standard 1 in. diameter quartz tube furnace for 30 min at  $550^\circ\text{C}$  with the feeding of  $\text{H}_2$  (100 sccm) and Ar (100 sccm) at ambient pressure. The  $\text{H}_2$  gas was then turned off, while  $\text{CH}_4$  (50 sccm) and  $\text{NH}_3$  (50 sccm) were introduced. The furnace temperature was raised to  $750^\circ\text{C}$  and the reaction was allowed to proceed for 30 min. The samples were fast-cooled to room temperature by quickly removing the sample from the hot zone of furnace under the protection of flowing Ar, using a magnetic rod. The sample was then leached in  $0.5 \text{ M H}_2\text{SO}_4$  at  $80^\circ\text{C}$  for 5 h, washed with distilled water 5 times, collected by magnetic separation using magnet cube and dried at  $60^\circ\text{C}$  under vacuum (140 Torr) for 12 h. To prepare the control sample of Co@G, it was subjected to the same synthetic procedures but without the flow of  $\text{NH}_3$  in the second step of the CVD process. To prepare NG, all the treatments were the same as those for N-Co@G but with no addition of Co salt in the hydrothermal reaction. To prepare N-Fe@G,  $\text{CoCl}_2$  was replaced by the same molar amount of  $\text{FeCl}_2$  during the hydrothermal reaction with all the other treatments kept the same.

**Characterization.** A JEOL 6500F Scanning Electron Microscope (SEM) was used to examine the morphology with porous features of the samples. A JEOL 2010 high resolution transmission electron microscope (HRTEM) was used to study the morphologic and structural characteristics of the samples. Chemical compositions and elemental oxidation states of the samples were investigated by XPS, which were taken on a PHI Quanta X-ray microprobe. An Al anode at 25 W was used as an X-ray source with a pass energy of  $26.00 \text{ eV}$ ,  $45^\circ$  take off angle, and a  $100 \mu\text{m}$  beam size. A pass energy of  $140 \text{ eV}$  was used for the survey and  $26 \text{ eV}$  for atomic concentration. XRD was carried out on a Rigaku D/Max Ultima II using  $\text{Cu K}\alpha$  radiation.

**Electrochemical measurement.** The electrochemical measurements were performed on a potentiostat (CHI 608D, CH Instruments, USA) using a three-electrode cell system. To prepare the working electrode, 4 mg catalyst and  $80 \mu\text{L}$  of 5 wt % Nafion solution were dispersed in 1 mL of 4:1 v/v water/ethanol by bath-sonication until a homogeneous suspension was formed. Then  $5 \mu\text{L}$  of the above catalyst suspension was drop-cast onto a glassy carbon electrode (3 mm in diameter) to give a mass loading of  $285 \mu\text{g cm}^{-2}$ . For a counter electrode, a Pt wire was used. For a reference electrode in acidic electrolyte ( $0.5 \text{ M H}_2\text{SO}_4$ ),  $\text{K}_2\text{SO}_4$  saturated  $\text{Hg}/\text{HgSO}_4$  electrode

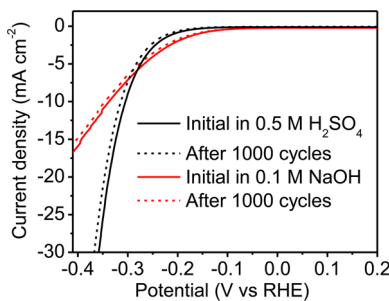


**Figure 5.** Polarization curves recorded at  $5 \text{ mV s}^{-1}$  for N-Co@G before and after cycling (in both acid and base) nearly overlap with only a small overpotential increase ( $<10 \text{ mV}$ ), suggesting its superior stability.

polarization curves recorded before and after cycling (in both acid and base) nearly overlap with only a small overpotential increase ( $<10 \text{ mV}$ ), suggesting its superior stability.

## CONCLUSION

In summary, we have reported the synthesis of nitrogen-enriched nanoparticles embedded in carbon spheres on graphene sheets (N-Co@G) by hydrothermal treatment,

(CH Instruments) was used and all potentials were referenced to a reversible hydrogen electrode (RHE) by adding a value of  $(0.67 + 0.059 \times \text{pH})$ . For testing in alkaline electrolyte (0.1 M NaOH), Hg/HgO (0.1 M NaOH) (CH Instruments) electrode was used and all potentials were referenced to RHE by adding a value of  $(0.165 + 0.059 \times \text{pH})$ . A flow of H<sub>2</sub> was maintained for 20 min before testing was started. Linear sweep voltammetry (LSV) polarization curves were performed at scan rate of 5 mV s<sup>-1</sup> and all the polarization curves were *iR*-corrected. EIS were carried out at both open circuit potential and 200 mV overpotential within the frequency range of 0.1 to 100 kHz with an a.c. voltage of 10 mV.

## ■ ASSOCIATED CONTENT

### § Supporting Information

Supplementary figures and tables. This material is available free of charge via the Internet at <http://pubs.acs.org>.

## ■ AUTHOR INFORMATION

### Corresponding Author

\*E-mail: tour@rice.edu.

### Notes

The authors declare no competing financial interest.

## ■ ACKNOWLEDGMENTS

Funding was provided by the AFOSR MURI program (FA9550-12-1-0035), and AFOSR (FA9550-14-1-0111). We also thank the Peter M. and Ruth L. Nicholas Post-Doctoral Fellowship of the Smalley Institute for Nanoscale Science and Technology for financial support (Y. Yang).

## ■ REFERENCES

- (1) Dresselhaus, M. S.; Thomas, I. L. *Nature* **2001**, *414*, 332–337.
- (2) Lewis, N. S.; Nocera, D. G. *Proc. Natl. Acad. Sci. U. S. A.* **2006**, *103*, 15729–15735.
- (3) Walter, M. G.; Warren, E. L.; McKone, J. R.; Boettcher, S. W.; Mi, Q.; Santori, E. A.; Lewis, N. S. *Chem. Rev.* **2010**, *110*, 6446–6473.
- (4) Voiry, D.; Yamaguchi, H.; Li, J.; Silva, R.; Alves, D. C. B.; Fujita, T.; Chen, M.; Asefa, T.; Shenoy, V. B.; Eda, G.; Chhowalla, M. *Nat. Mater.* **2013**, *12*, 850–855.
- (5) Voiry, D.; Salehi, M.; Silva, R.; Fujita, T.; Chen, M.; Asefa, T.; Shenoy, V. B.; Eda, G.; Chhowalla, M. *Nano Lett.* **2013**, *13*, 6222–6227.
- (6) Liao, L.; Zhu, J.; Bian, X.; Zhu, L.; Scanlon, M. D.; Girault, H. H.; Liu, B. *Adv. Funct. Mater.* **2013**, *23*, 5326–5333.
- (7) Shin, H. S.; Yang, J. *J. Mater. Chem. A* **2014**, *2*, 5979–5985.
- (8) Kong, D.; Wang, H.; Cha, J. J.; Pasta, M.; Koski, K. J.; Yao, J.; Cui, Y. *Nano Lett.* **2013**, *13*, 1341–1347.
- (9) Wang, H.; Kong, D.; Johanes, P.; Cha, J. J.; Zheng, G.; Yan, K.; Liu, N.; Cui, Y. *Nano Lett.* **2013**, *13*, 3426–3433.
- (10) Faber, M. S.; Dziedzic, R.; Lukowski, M. A.; Kaiser, N. S.; Ding, Q.; Jin, S. *J. Am. Chem. Soc.* **2014**, *136*, 10053–10061.
- (11) Kong, D.; Cha, J.; Wang, H.; Lee, H. R.; Cui, Y. *Energy Environ. Sci.* **2013**, *6*, 3553–3558.
- (12) Kong, D.; Wang, H.; Lu, Z.; Cui, Y. *J. Am. Chem. Soc.* **2014**, *136*, 4897–4900.
- (13) Liu, Q.; Tian, J.; Cui, W.; Jiang, P.; Cheng, N.; Asiri, A. M.; Sun, X. *Angew. Chem., Int. Ed.* **2014**, *53*, 6710–6714.
- (14) Tian, J.; Liu, Q.; Asiri, A. M.; Sun, X. *J. Am. Chem. Soc.* **2014**, *136*, 7587–7590.
- (15) Popczun, E. J.; McKone, J. R.; Read, C. G.; Biacchi, A. J.; Wiltrot, A. M.; Lewis, N. S.; Schaak, R. E. *J. Am. Chem. Soc.* **2013**, *135*, 9267–9270.
- (16) Feng, L.; Vrubel, H.; Bensimon, M.; Hu, X. *Phys. Chem. Chem. Phys.* **2014**, *16*, 5917–5921.
- (17) Tian, J.; Liu, Q.; Cheng, N.; Asiri, A. M.; Sun, X. *Angew. Chem., Int. Ed.* **2014**, *53*, 9557–9581.
- (18) Wang, X.; Xiao, P.; Thia, L.; Alam, Sk. M.; Lim, R. J.; Ge, X.; Wang, J. Y.; Lim, K. H. *Energy Environ. Sci.* **2014**, *7*, 2624–2629.
- (19) Vrubel, H.; Hu, X. *Angew. Chem.* **2012**, *124*, 12875–12878.
- (20) Liao, L.; Wang, S.; Xiao, J.; Bian, X.; Zhang, Y.; Scanlon, M. D.; Hu, X.; Tang, Y.; Girault, H. H.; Liu, B. *Energy Environ. Sci.* **2014**, *7*, 387–392.
- (21) Hunt, S. T.; Nimmanwudipong, T.; Román-Leshkov, Y. *Angew. Chem., Int. Ed.* **2014**, *53*, 5131–5136.
- (22) Los, P.; Lasia, A. *J. Electroanal. Chem.* **1992**, *333*, 115–125.
- (23) Chakrapani, V.; Thangala, J.; Sunkara, M. K. *Int. J. Hydrogen Energy* **2009**, *34*, 9050–9059.
- (24) Cao, B.; Veith, G. M.; Neufeind, J. C.; Adzic, R. R.; Khalifah, P. *J. Am. Chem. Soc.* **2013**, *135*, 19186–19192.
- (25) Zheng, Y.; Jiao, Y.; Zhu, Y.; Li, L. H.; Han, Y.; Chen, Y.; Du, A.; Jaroniec, M.; Qiao, S. Z. *Nat. Commun.* **2014**, *5*, 3783.
- (26) Zheng, Y.; Jiao, Y.; Li, L. H.; Xing, T.; Chen, Y.; Jaroniec, M.; Qiao, S. Z. *ACS Nano* **2014**, *8*, 5290–5296.
- (27) Fei, H.; Peng, Z.; Yang, Y.; Li, L.; Raji, A. R. O.; Samuel, E. L. G.; Tour, J. M. *Chem. Commun.* **2014**, *50*, 7117–7119.
- (28) Lee, S.; Cho, Y.; Song, H. K.; Lee, K. T.; Cho, J. *Angew. Chem., Int. Ed.* **2012**, *51*, 8748–8752.
- (29) Wang, Z.; Luan, D.; Madhavi, S.; Hu, Y.; Lou, X. W. *Energy Environ. Sci.* **2012**, *5*, 5252–5256.
- (30) Cheng, L.; Yan, J.; Zhu, G. N.; Luo, J. Y.; Wang, C. X.; Xia, Y. Y. *J. Mater. Chem.* **2010**, *20*, 595–602.
- (31) Li, H.; Zhou, H. *Chem. Commun.* **2012**, *48*, 1201–1217.
- (32) Inagaki, M. *Carbon* **2012**, *50*, 3247–3266.
- (33) Hu, Y.; Jensen, J. O.; Zhang, W.; Cleemann, L. N.; Xing, W.; Bjerrum, N. J.; Li, Q. *Angew. Chem., Int. Ed.* **2014**, *53*, 3675–3679.
- (34) Wen, Z.; Ci, S.; Zhang, F.; Feng, X.; Cui, S.; Mao, S.; Luo, S.; He, Z.; Chen, J. *Adv. Mater.* **2012**, *24*, 1399–1404.
- (35) Zou, X.; Huang, X.; Goswami, A.; Silva, R.; Sathe, B. R.; Mikmeková, E.; Asefa, T. *Angew. Chem., Int. Ed.* **2014**, *53*, 4372–4376.
- (36) Deng, J.; Ren, P.; Deng, D.; Yu, L.; Yang, F.; Bao, X. *Energy Environ. Sci.* **2014**, *7*, 1919–1923.
- (37) Zhou, W.; Zhou, Y.; Yang, L.; Huang, J.; Ke, Y.; Zhou, K.; Li, L.; Chen, S. *J. Mater. Chem. A* **2014**, DOI: 10.1039/C4TA06284A.
- (38) Deng, D.; Yu, L.; Chen, X.; Wang, G.; Jin, L.; Pan, X.; Deng, J.; Sun, G.; Bao, X. *Angew. Chem., Int. Ed.* **2013**, *52*, 371–375.
- (39) Deng, J.; Yu, L.; Deng, D.; Chen, X.; Yang, F.; Bao, X. *J. Mater. Chem. A* **2013**, *1*, 14868–14873.
- (40) Deng, J.; Ren, P.; Deng, D.; Bao, X. *Angew. Chem., Int. Ed.* **2015**, *54*, 2100–2104.
- (41) Tavakkoli, M.; Kallio, T.; Reynaud, O.; Nasibulin, A. G.; Johans, C.; Sainio, J.; Jiang, H.; Kauppinen, E. I.; Laasonen, K. *Angew. Chem., Int. Ed.* **2015**, DOI: 10.1002/anie.2014111450.
- (42) Zhou, W.; Zhou, J.; Zhou, Y.; Lu, J.; Zhou, K.; Yang, L.; Tang, Z.; Li, L.; Chen, S. *Chem. Mater.* **2015**, DOI: 10.1021/acs.chemmater.5b00331.
- (43) Zheng, X.; Deng, J.; Wang, N.; Deng, D.; Zhang, W.-H.; Bao, X.; Li, C. *Angew. Chem., Int. Ed.* **2014**, *53*, 7023–7027.
- (44) Yin, H.; Zhao, S.; Wan, J.; Tang, H.; Chang, L.; He, L.; Zhao, H.; Gao, Y.; Tang, Z. *Adv. Mater.* **2013**, *25*, 6270–6276.
- (45) Fei, H.; Peng, Z.; Li, L.; Yang, Y.; Lu, W.; Samuel, E. G.; Fan, X.; Tour, J. M. *Nano Res.* **2014**, *7*, 1–9.
- (46) Wang, H.; Maiyalagan, T.; Wang, X. *ACS Catal.* **2012**, *2*, 781–794.
- (47) McCrory, C. C. L.; Jung, S.; Peters, J. C.; Jaramillo, T. F. *J. Am. Chem. Soc.* **2013**, *135*, 16977–16987.
- (48) Li, Y.; Wang, H.; Xie, L.; Liang, Y.; Hong, G.; Dai, H. J. *Am. Chem. Soc.* **2011**, *133*, 7296–7299.
- (49) Luo, J.; Im, J.; Mayer, M.; Schreier, M.; Nazeeruddin, M.; Park, N.; Tilley, S.; Fan, H.; Gratzel, M. *Science* **2014**, *345*, 1593–1596.
- (50) Marcano, D. C.; Kosynkin, D. V.; Berlin, J. M.; Sinitskii, A.; Sun, Z.; Slesarev, A.; Alemany, L. B.; Lu, W.; Tour, J. M. *ACS Nano* **2010**, *4*, 4806–4814.